Nanoparticle-enabled innate immune stimulation activates endogenous tumor-infiltrating T cells with broad antigen specificities

Qian Yin[a], Wong Yu[b,c], Caitlin L. Grzeskowiak[d], Jing Li[a], Huang Huang[e], Jing Guo[b], Liang Chen[a], Feng Wang[e], Fan Zhao[b,1], Lotta von Boehmer[a], Thomas J. Metzner[f], John T. Leppert[f], Yueh-hsiu Chien[a,b], Calvin J. Kuo[d], and Mark M. Davis[a,b,e,2]

[a]Institute for Immunity, Transplantation and Infection, School of Medicine, Stanford University, Stanford, CA 94305; [b]Department of Microbiology and Immunology, School of Medicine, Stanford University, Stanford, CA 94305; [c]Division of Allergy, Immunology and Rheumatology, Department of Pediatrics, Sean N. Parker Center for Allergy and Asthma Research, Stanford University, Stanford, CA 94305; [d]Division of Hematology, Department of Medicine, School of Medicine, Stanford University, Stanford, CA 94305; [e]HHMI, Stanford University School of Medicine, Stanford, CA 94305; and [f]Department of Urology, School of Medicine, Stanford University, Stanford, CA 94305

Contributed by Mark M. Davis, April 6, 2021 (sent for review August 13, 2020; reviewed by Paul M. Allen and Olivera J. Finn)

Tumors are often infiltrated by T lymphocytes recognizing either self- or mutated antigens but are generally inactive, although they often show signs of prior clonal expansion. Hypothesizing that this may be due to peripheral tolerance, we formulated nanoparticles containing innate immune stimulants that we found were sufficient to activate self-specific CD8$^+$ T cells and injected them into two different mouse tumor models, B16F10 and MC38. These nanoparticles robustly activated and/or expanded antigen-specific CD8$^+$ tumor-infiltrating T cells, along with a decrease in regulatory CD4$^+$ T cells and an increase in Interleukin-17 producers, resulting in significant tumor growth retardation or elimination and the establishment of immune memory in surviving mice. Furthermore, nanoparticles with modification of stimulating human T cells enabled the robust activation of endogenous T cells in patient-derived tumor organoids. These results indicate that breaking peripheral tolerance without regard to the antigen specificity creates a promising pathway for cancer immunotherapy.

cancer immunotherapy | self-antigen–specific tumor-infiltrating T cells | peripheral tolerance | innate immune stimulation | nanoparticles

Cancer immunotherapy has held out the promise of harnessing a patient's own immune system to attack cancer cells for many years. While checkpoint inhibitors and chimeric antigen receptor T cells have triggered long-term remissions in some patients, many more do not respond or have a recurrence, hence the need for additional approaches (1–5). Tumor-infiltrating T cells (TILs), which are found in approximately one-third of the most common tumor types (6, 7), are often either self-antigen or mutated antigen (neoantigen) specific (8, 9), although recent analyses have also documented T cells specific for infectious diseases (10, 11). Self-antigen–specific T cells are particular characteristics of tumor types with lower tumor mutational burden and poorer outcomes (12–14), suggesting that activating these T cells might be particularly beneficial for immunotherapy. Although for many years, it has been thought that almost all self-antigen–specific T cells were deleted in the thymus due to negative selection (15, 16), our own studies of healthy human blood donors (17, 18) and parallel work in mice (19) have shown that only a fraction (~70 to 0%) of the self-specific T cells is actually eliminated. We also observed profound differences in the activation requirements in the self-antigen–specific vs. foreign antigen-specific T cells—while the latter could be stimulated with cognate antigen plus anti-CD28 and Interleukin (IL)-2, the former could not. Since anti-CD3 could stimulate both cells in vitro, the results suggested that the self-specific T cells were not anergic, but rather, lacked some other signals. Reasoning that these signals were likely related to those triggered by an active infection, as suggested by the classical work of Ohashi and colleagues (20) and others, we surveyed a range of agonists for pattern recognition receptors (PRRs). We found that just two, the lipoprotein (Pam3CysSerLys4 [Pam3CSK4]), an agonist for the Toll-like receptor 1/2 heterodimer (TLR1/2), and muramyl dipeptide (L18-MDP), an agonist for the cytosolic nucleotide-binding oligomerization domain receptor 2 (NOD2), were sufficient to stimulate self-antigen–specific CD8$^+$ T cells in vitro as efficiently as foreign antigen-specific CD8$^+$ T cells, where both were in the presence of IL-2 and anti-CD28. These results support the hypothesis that self-specific T cells are held in a nonreactive state unless activated by an infection, with its mobilization of the innate immune system.

In our previous human colon carcinoma studies (21, 22), both CD4$^+$ and CD8$^+$ TILs showed extensive clonal expansion, indicating that they had been very active at one point but likely were no longer. Consistent with this aborted response phenomenon is earlier work showing that in metastatic melanoma patients, tumor-associated

Significance

Tumors are often infiltrated by T lymphocytes recognizing either self- or mutated antigens but are generally inactive. Self-specific CD8$^+$ T cells are particular characteristics of tumor types with lower tumor mutation burden and poorer outcomes. Unlike foreign-specific T cells, they have been curiously resistant to stimulation with cognate antigens. We developed an innate immunity-stimulating nanoparticle to activate tumor-infiltrating CD8$^+$ T cells recognizing both self- and neoantigens in a potent yet safe manner. This resulted in effective tumor growth inhibition or elimination in two murine tumor models and the activation of endogenous T cells in patient-derived tumor organoids across three cancer types. This strategy represents a promising pathway for broadly effective cancer immunotherapy.

Author contributions: Q.Y., W.Y., H.H., Y.-h.C., C.J.K., and M.M.D. designed research; Q.Y., W.Y., C.L.G., J.L., and J.G. performed research; F.Z. contributed new reagents/analytic tools; Q.Y., W.Y., C.L.G., J.L., J.G., L.C., and F.W. analyzed data; L.v.B., T.J.M., and J.T.L. assisted with human sample collection; and Q.Y. and M.M.D. wrote the paper.

Reviewers: P.M.A., Washington University School of Medicine; and O.J.F., University of Pittsburgh School of Medicine.

Competing interest statement: Q.Y., W.Y., and M.M.D. are inventors on a patent application that describes the use of these nanoparticles for cancer immunotherapy.

[1]Present address: Discovery & Translational Immunology, Cue Biopharma, Inc., Cambridge, MA 02139.

[2]To whom correspondence may be addressed. Email: mmdavis@stanford.edu.

This article contains supporting information online at https://www.pnas.org/lookup/suppl/doi:10.1073/pnas.2016168118/-/DCSupplemental.

Published May 21, 2021.

"self"-antigen–specific $CD8^+$ T cells recognizing peptides from melanoma antigen recognized by T cells 1 (MART-1), gp100, and tyrosinase are present in the circulation in much higher frequency than baseline but in an inactive or only partially active state compared with virus-specific T cells in the same patients (12). Also suggesting an arrest in activity are the results of cell transfer experiments, where Yee et al. (23) transferred large numbers of MART-1–specific $CD8^+$ T cells in melanoma patients and observed only short-term activity arrested after a few days.

Thus, we hypothesized that tumor-infiltrating self-specific and perhaps even neoantigen-specific $CD8^+$ T cells could be in a quiescent state similar to that of self-specific T cells in the periphery, and breaking this type of peripheral tolerance might activate these cells and trigger antitumor immunity. However, if given systemically, many of these agents will elicit severe inflammatory toxicities (24, 25). The systemic activation of self-specific $CD8^+$ T cells in particular would also likely induce autoimmunity (26). To address these issues, we developed a biodegradable nanoparticle (NP) platform, covalently conjugated with an anti-CD28 antibody (Ab) and capable of delivering IL-2, Pam3CSK4, and L18-MDP in a sustained manner to achieve continuous local stimulation in the tumor microenvironment and minimize the side effects that would likely result from systemic exposure.

Using this NP, we first demonstrated that self-specific $CD8^+$ T cells isolated from either peripheral blood mononuclear cells (PBMCs) of healthy humans or the tumor-draining lymph nodes of B16F10 melanoma-inoculated mice could be expanded in vitro with NP-enabled stimulation in the presence of relevant self-peptides. Second, we showed that the repeated injection of these NPs into mice bearing either the B16F10 melanoma or MC38 colon carcinoma could generally activate both self-antigen and neoantigen-specific TILs, leading to significant retardation of tumor growth and prolongation of survival in these treated mice. Some mice totally rejected tumors and were completely resistant to tumor reinoculation, indicating that their immune system has acquired systemic "memory." Evidence suggests that this antitumor activity is, at least in part, due to a reduction in the number and suppressive activity of regulatory T cells (Tregs) and the maturation of antigen-presenting cells (APCs). We further demonstrated that this approach could stimulate human TILs in patient-derived tumor organoids from three different cancer types, even those unresponsive to checkpoint blockades. Altogether, these results indicate that breaking peripheral tolerance with a combination of innate immune stimulants to activate both self-antigen– and neoantigen-specific TILs represents a broadly applicable and effective strategy for cancer immunotherapy.

Results

In Vitro Activation and/or Expansion of Self-Specific $CD8^+$ T Cells from Human PBMCs by NPs. Inspired by the prior work of Ohashi and colleagues (20), who showed that T cell receptor (TCR) transgenic T cells specific for a viral antigen expressed in beta islet cells of mice only caused tissue destruction when infected by a virus expressing that antigen, we hypothesized that an innate immune response in addition to an adaptive one is necessary to "break" peripheral tolerance and enables the activation of self-specific T cells. Therefore, we screened a panel of innate immune agonists (*SI Appendix*, Table S1) and found that Pam3CSK4, an agonist for TLR1/2 heterodimer, and L18-MDP, an agonist for the NOD2, among all the screened agonists were the most effective in activating self-specific $CD8^+$ T cells from healthy human blood donors (*SI Appendix*, Fig. S1). Specifically, we incubated healthy human PBMCs with or without Pam3CSK4 and L18-MDP in the presence of four self-peptides (Table 1, labeled by *) and an anti-CD28 Ab plus IL-2. As shown in Fig. 1*A*, nonstimulated self-tetramer$^+$$CD8^+$ T cells expressed very low CD25 expression, while with the simulation of TLR1/2 and NOD2 agonists, the CD25 expression of self-tetramer$^+$$CD8^+$ T cells was significantly up-regulated.

Table 1. Self-specific peptides and foreign-specific peptides used for tetramer staining for $CD8^+$ T cells from human blood donor PBMCs

Self peptide pool	Foreign peptide pool
FBA (216:224) ALSDHHIYL *	HBV core (18:27) FLPSDFFPSV
KER (307:315) ALLNIKVKL *	HCV ns5b (2594:2602) ALYDVVTKL
GAD65 (114:123) VMNILLQYVV *#	HIV p17 gag (77:85) SLYNTVATL
GAD65 (536:545) RMMEYGTTMV #	HIV gag (1:10) FLGKIWPSYK
IA-2 (805:813) VIVMLTPLV #	HIV gp160 (814:822) LLNATDIAV
IGRP (215:223) FLFAVGFYL #	HIV protease (76:84) LVGPTPVNI
IGRP (265:273) VLFGLGFAI #	HIV rt (127:135) YTAFTIPSV
MBP (111:119) SLSRFSWGA #	HIV vpr (59:67) AIIRILQQL
PDC-E2 (159:167) KLSEGDLLA #	HIV rt (179:187) VIYQYMDDL
PPI (2:10) ALWMRLLPL *#	
PPI (2:11) ALWMRLLPLL #	
PPI (6:14) RLLPLLALL #	
PPI (15:24) ALWGPDPAAA #	
PPI (34:42) HLVEALYLV #	
PPI (76:84) SLQPLALEG #	
ppIAPP(5:13) KLQVFLIVL #	
ZnT8 (153:61) VVTGVLVYL #	
ZnT8 (266:74) ILKDFSILL #	

HBV: hepatitis B virus; HCV: hepatitis C virus; HIV: human immunodeficiency virus. (*peptides for Fig. 1A; # peptides for Fig. 1B).

In order to safely use the identified stimulants (combined Pam3CSK4 and L18-MDP plus anti-CD28 Ab and IL-2) to in vivo activate self-specific $CD8^+$ TILs, we formulated an anti-CD28 Ab functionalized NP enabling the persistent release of IL-2, Pam3CSK4, and L18-MDP in the tumor microenvironment. Specifically, IL-2, Pam3CSK4, and L18-MDP were mixed with poly(ethylene glycol)-*b*-poly(lactic-*co*-glycolic acid) (PEG-PLGA) and PLGA-PEG-maleimide polymers and self-assembled into 177-nm-sized NPs through the double-emulsion method (27, 28) (*SI Appendix*, Fig. S2*A*). The anti-CD28 Ab was then conjugated on the surface of these NPs via thiol-maleimide conjugation. Upon dissolution and degradation of NPs in the physiological condition, the encapsulated IL-2, Pam3CSK4, and L18-MDP slowly released from NPs (*SI Appendix*, Fig. S2 *B* and *C*).

We first evaluated the capacity of these NPs to in vitro stimulate self-specific $CD8^+$ T cells from healthy human PBMCs. We sorted self-specific $CD8^+$ T cells from the PBMCs of healthy humans using pooled HLA-A*0201 tetramers loaded with 16 self-peptides (Table 1, labeled by #) and cultured them with either a mixture of the soluble stimulants (Fig. 1 *B*, *Top*) or NPs (Fig. 1 *B*, *Bottom*) in the presence of the same peptides used for tetramer staining. The foreign-specific $CD8^+$ T cells were also sorted with pooled HLA-A*0201 tetramers loaded with nine foreign peptides (Table 1) and cultured under the same conditions as a control (*SI Appendix*, Fig. S3). The CD25 expression on the self-specific $CD8^+$ T cells cocultured with NPs was up-regulated in an equivalent manner as that on the cells stimulated with the soluble mixture (Fig. 1 *B*, *Left*), demonstrating that these molecules were equally active in the NP format. CFSE dilutions also confirmed that self-specific T cells coincubated with the NPs proliferated equally well as cells coincubated with the soluble mixture (Fig. 1 *B*, *Right*). In the case of foreign-specific $CD8^+$ T cells, we also found that the NPs are capable of activating these cells and stimulating them to proliferate (*SI Appendix*, Fig. S3).

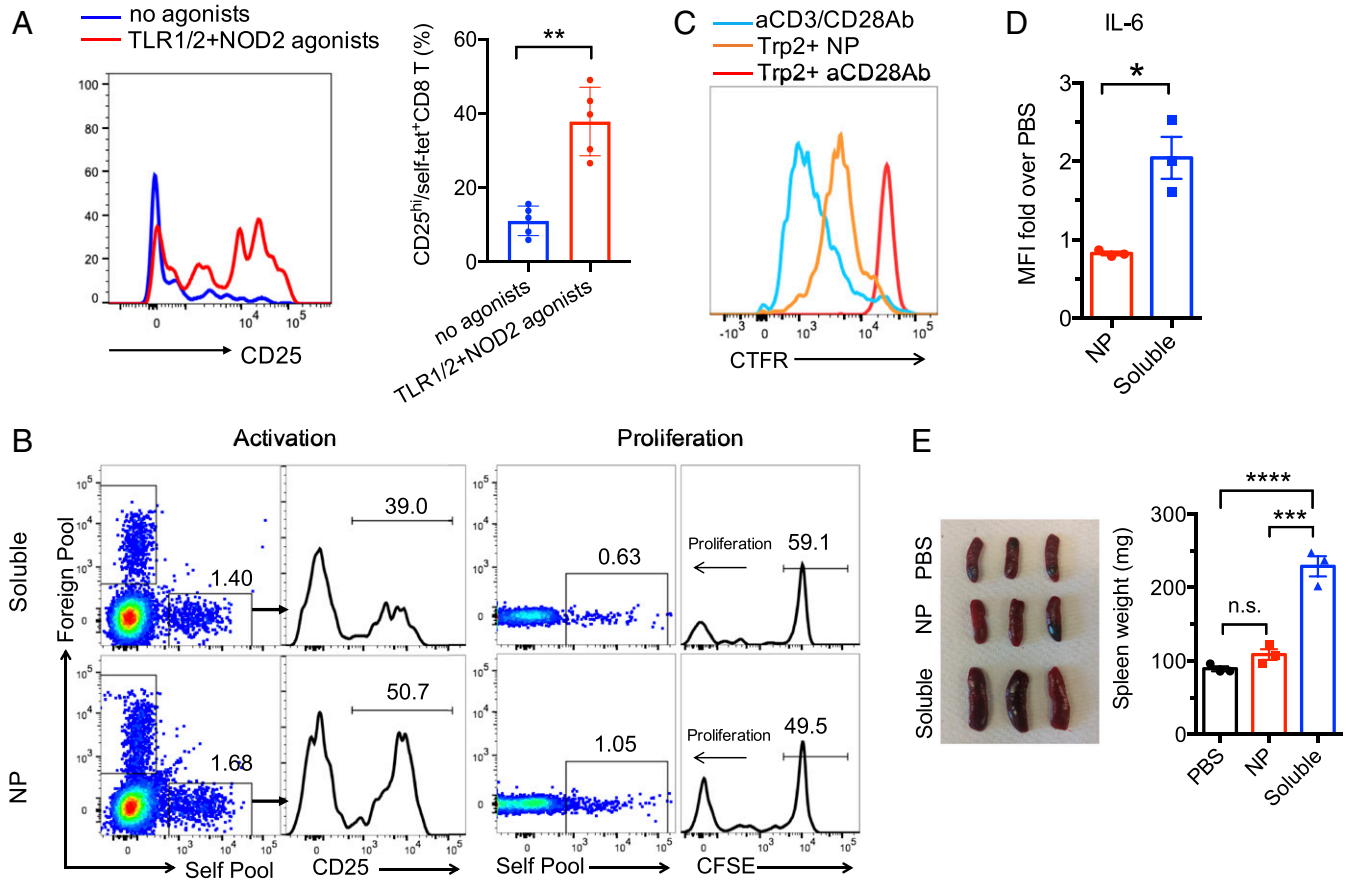

Fig. 1. Loaded NPs promote self-specific CD8$^+$ T cells expansion and activation in vitro and reduce systemic toxicities of a soluble stimulant mixture in vivo. (*A*) The TLR1/2 agonist and NOD2 agonist stimulated self-antigen–specific CD8$^+$ T cells in healthy human PBMCs ($n = 5$). In this assay, PBMCs were directly cultured with Pam3CSK4 and L18-MDP in the presence of pooled self-specific peptides, anti-CD28 Ab, and IL-2 and stained with pooled HLA-A*0201 tetramers at day 7. The T cell activation was characterized by measuring the percentage increase in CD25 expression of self-tetramer$^+$CD8$^+$ T cells. Data are means ± SD. Data were analyzed by unpaired *t* test with Welch's correction. $^{**}P < 0.01$. (*B*) The representative flow cytometric analysis showing the proliferation and activation of self-specific CD8$^+$ T cells from healthy blood donors after stimulation with a mixture of soluble stimulants (*Top*) or NPs (*Bottom*) in the presence of pooled self-peptides at day 7.5. The soluble stimulant mixture includes IL-2, Pam3CSK4, L18-MDP, and anti-CD28 Ab. The NPs were loaded with equivalent dose of IL-2, Pam3CSK4, and L18-MDP, and anti-CD28 Abs conjugated to their surfaces. For the proliferation assay, self-specific CD8$^+$ T cells were sorted by pooled HLA-A*0201 tetramers loaded with self-specific peptides, CFSE labeled, and cultured under the different stimulation conditions in the presence of autologous feeder PBMCs with the same peptides used for tetramer sorting. T cell proliferation was characterized by measuring the CFSE dilution of tetramer$^+$CD8$^+$ T cells. The most brightly CFSE-stained cells are not proliferating. For the activation assay, PBMCs were directly cultured under the stimulation conditions in the presence of pooled self-specific peptides and stained with pooled HLA-A*0201 tetramers at day 7.5. The T cell activation was characterized by measuring the percentage increase in CD25 expression of self-tetramer$^+$CD8$^+$ T cells. Data are representative of three human individuals. (*C*) Representative flow cytometric analysis showing the proliferation of TRP2-specific CD8$^+$ T cells isolated from B16F10 melanoma-bearing mice. CD8$^+$ T cells were sorted from tumor-draining lymph nodes of B16F10 melanoma-bearing mice, labeled with cell trace far red (CTFR), and stimulated with different stimulants such as anti-CD28 Ab plus TRP2 peptide, anti-CD3/CD28 Ab, or NPs plus TRP2 peptide. Data are representative of two independent experiments. (*D*) The concentration of IL-6 in the serum of C57BL/6 mice 2 h after a single subcutaneous injection of a soluble stimulant mixture or NPs ($n = 3$). The data were represented as fold change of mean fluorescence intensity (MFI) over the PBS group. (*E*) Splenomegaly assessment of C57BL/6 mice on day 7 received three injections (day 1, day 3, and day 5) of PBS, NP, or a soluble stimulant mixture. Soluble is short for a soluble stimulant mixture ($n = 3$). Data are means ± SEM. Data were analyzed by one-way ANOVA with Bonferroni posttest. n.s. not significant; $^*P < 0.05$; $^{**}P < 0.01$; $^{***}P < 0.001$; $^{****}P < 0.0001$.

Apparently "Exhausted" Self-Specific CD8$^+$ T Cells Are Enriched in a Murine Tumor Model but Can Be Activated by NPs. To investigate whether these NPs might be able to stimulate self-specific CD8$^+$ T cells in a tumor, we first characterized the phenotype and function of CD8$^+$ T cells recognizing tyrosinase-related protein 2 (TRP2) (13), a dominant self-melanocyte differentiation antigen present in the poorly immunogenic B16F10 murine melanoma model. As reported previously (29), we found that TRP2-specific CD8$^+$ (denoted as TRP2$^+$CD8$^+$) T cells are notably enriched in tumor tissues (30.1%) in contrast to lymph node (<1%) and spleen (<1%) 11 d posttumor inoculation (*SI Appendix*, Fig. S4*A*). Interestingly, these TRP2$^+$CD8$^+$ TILs exhibited a distinctly exhausted phenotype compared with non-TRP2–specific (TRP2$^-$CD8$^+$) TILs, in that they had increased programmed cell death protein 1 (PD-1) expression (*SI Appendix*, Fig. S4*B*). Moreover, the substantial decrease in interferon (IFN)-γ production of CD8$^+$ TILs, from 10.0% at day 11 to 5.03% at day 17, after ex vivo stimulation with TRP2 peptide suggests that they gradually lost functionality during tumor progression (*SI Appendix*, Fig. S4*C*).

To determine whether these TRP2$^+$CD8$^+$ T cells could be activated with our NP-enabled innate stimulation, we first stimulated them with the NPs in vitro. Given the limited number of T cells infiltrating into B16F10 tumors, we alternatively sorted CD8$^+$ T cells from the tumor-draining lymph nodes when the tumor was fully established. The sorted CD8$^+$ T cells were cultured with TRP2 peptides under different conditions in the presence of JAWSII APCs. We found that the cells stimulated

solely with the anti-CD28 Ab showed minimal proliferation, whereas the cells treated with the fully loaded NPs showed robust proliferation (Fig. 1*C*). To further elucidate the importance of each stimulatory component incorporated into the NPs, we formulated a series of NPs with one component excluded (*SI Appendix*, Table S2) and tested the effects of these NPs on the proliferation of TRP2$^+$ CD8$^+$ T cells isolated from tumor-draining lymph nodes. The results revealed that only NPs containing all four stimulants (IL-2, Pam3CSK4, L18-MDP, and the anti-CD28 Ab) drives the proliferation of TRP2$^+$ T cells to the greatest extent (*SI Appendix*, Fig. S5). Therefore, all future studies were carried out using the NPs containing all four components.

NP Stimulation Minimizes Systemic Immune Toxicity. Before applying these NPs to in vivo activate CD8$^+$ TILs, we first evaluated systemic toxicity by subcutaneously injecting the NPs into C57BL/6

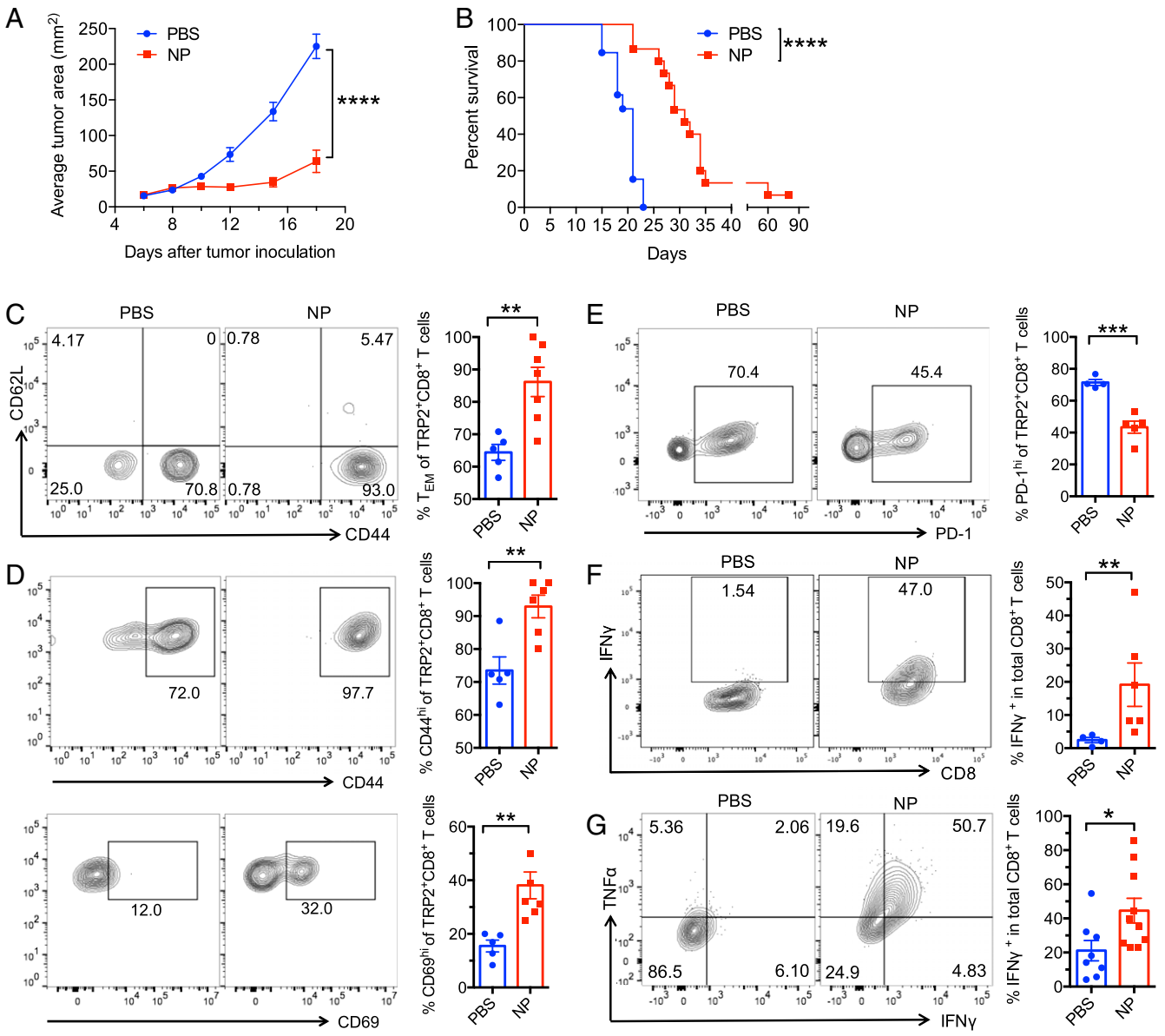

Fig. 2. Loaded NPs activate endogenous TRP2-tetramer$^+$CD8$^+$ TILs in vivo, leading to suppression of tumor growth, prolongation of overall survival, and establishment of protective memory in B16F10 melanoma. (*A*) The average tumor growth curve of B16F10 melanoma-bearing mice (n = 10) who received three treatments of PBS or NPs on days 5, 11, and 17. Data were analyzed by two-way ANOVA. ****P < 0.0001. (*B*) The percentage survival of B16F10 melanoma-bearing mice (n = 13 to 15) after three treatments was monitored over time. Data were analyzed by log-rank (Mantel–Cox) test. ****P < 0.0001. (*C*) NP drives endogenous TRP2-tetramer$^+$CD8$^+$ T cell response strongly biased toward effector memory (T_{EM}: CD44^{hi}CD62L^{lo}CD8$^+$ T) populations (flow plot [*Left*]; quantification [*Right*]) on day 17 (n = 5 to 7). (*D*) The representative flow cytometry plot (*Left*) and the corresponding quantification (*Right*) of surface activation marker staining (CD44 and CD69) of TRP2-tetramer$^+$CD8$^+$ T cells from freshly isolated B16F10 melanoma on day 17 (n = 5 to 7). (*E*) The representative flow cytometry plot (*Left*) and the corresponding quantification (*Right*) of PD-1 staining of TRP2-tetramer$^+$CD8$^+$ T cells from freshly isolated B16F10 melanoma on day 17 (n = 4 to 5). In Fig. *C–E*, all the data are means ± SEM. Data were analyzed by unpaired t test with Welch's correction. *P < 0.05; **P < 0.01; ***P < 0.001. (*F*) The representative flow cytometry plot (*Left*) and the corresponding quantification (*Right*) of IFN-γ–producing TRP2-specific CD8$^+$ T cells after ex vivo stimulation of TRP2 peptide on day 17 (n = 4 to 6). (*G*) The representative flow cytometry plot (*Left*) and the corresponding quantification (*Right*) showing that NP increases the frequency of IFN-γ–producing CD8$^+$ T cells in total CD8$^+$ T cell population in B16F10 melanoma after ex vivo stimulation of cell stimulation mixture on day 17 (n = 8 to 10). In panels *F* and *G*, all the data are means ± SEM. Data were analyzed by Mann-Whitney test. *P < 0.05; **P < 0.01; ***P < 0.001.

mice. Phosphate-buffered saline (PBS) and a soluble stimulant mixture were used as controls. The soluble stimulant mixture rapidly diffused into circulation within 2 h after a single subcutaneous injection, leading to acute inflammation, characterized by elevated serum inflammatory cytokines of IL-6 (Fig. 1*D*). Repeated injections of the soluble stimulants mixture resulted in significantly enlarged spleens (splenomegaly) (Fig. 1*E*). In contrast, both single and repeated injections of the NPs loaded with these same compounds showed negligible systemic inflammation (Fig. 1 *D* and *E*).

In Vivo Activation of Endogenous Self-Specific CD8$^+$ TILs by NP Stimulation Elicits a Robust Antitumor Immune Response. When the B16F10 melanomas were fully established in the mice, we repeatedly injected these NPs into the tumors three times. The results show that NP treatment significantly slowed tumor growth and prolonged the overall survival (Fig. 2 *A* and *B*), while the soluble stimulant mixture showed a less effective effect compared with NPs (*SI Appendix*, Fig. S6*A*). This is likely due to the fact that the rapid diffusion of the soluble stimulant mixture limits the effective dose. The same treatment with blank NPs (no stimulants encapsulated or anti-CD28 Ab conjugated) did not affect tumor growth (*SI Appendix*, Fig. S6*B*). One of 15 of the NP-treated mice survived, with some vitiligo only at the injection site (*SI Appendix*, Fig. S6*C*), indicating the stimulation of an antimelanocyte response. This surviving mouse rejected the rechallenge with the same tumor line (*SI Appendix*, Fig. S6*D*).

We next analyzed the phenotype of T cells after NP treatment. This showed that NP stimulation drives the T cell response strongly toward effector memory (CD44^{hi}CD62L^{low}) T cells in the tumor (Fig. 2*C*). A significant up-regulation of CD44 and CD69 also indicated the activation of TRP2$^+$CD8$^+$ T cells after NP treatment (Fig. 2*D*). Importantly, we saw evidence that NP treatment restores the functionality of the self-specific CD8$^+$ T cells, as shown by the down-regulation of PD-1 expression of TRP2$^+$CD8$^+$ T cells (Fig. 2*E*) and the markedly enhanced IFN-γ production of CD8$^+$ T cells after stimulation with TRP2 peptide (Fig. 2*F*). We also characterized the phenotype and function of total tumor-infiltrating CD8$^+$ T cells regardless of antigen specificity. Flow cytometry analysis confirmed the effector or effector memory differentiation of total CD8$^+$ T cells after NP stimulation (*SI Appendix*, Fig. S6*E*). The enhanced IFN-γ production of CD8$^+$ T cells after stimulation with cell stimulation mixture was also observed (Fig. 2*G*), indicating that NPs could have a broad activation effect on the whole CD8$^+$ T cell repertoire in the tumor.

Activation of Neoantigen-Specific CD8$^+$ TILs. These results prompted us to further investigate whether NP stimulation impacts the tumor-infiltrating CD8$^+$ T cells recognizing neoantigens. We first evaluated the efficacy of NP treatment in murine MC38 colon carcinoma, a tumor model with a high frequency of mutations. Results revealed a strong therapeutic effect of NPs in this tumor model with a robust inhibition of tumor growth (Fig. 3*A*) and prolonged overall survival (Fig. 3*B*). Strikingly, NP treatment induced durable cures in 50% of the mice, and all of them rejected a second tumor challenge, indicating the establishment of effective immunological memory (Fig. 3*C*). We next examined the CD8$^+$ T cell response elicited by NP stimulation. In contrast to PBS treatment, intratumoral injection of NPs strongly drove total CD8$^+$ TILs toward an effector memory phenotype and led to markedly increased effector memory as well as tumor necrosis factor (TNF)-α– and IFN-γ–producing CD8$^+$ T cell populations in the tumor (Fig. 3 *D* and *E*). Further flow cytometry analysis showed a direct effect on one of the known neoantigen specificities in MC38 tumors, with a 2.4-fold increase in neoantigen (ASMTNMELM)-specific CD8$^+$ T cells from tumor-draining lymph nodes after NP treatment. In contrast, the frequency of these cells barely changed after NP treatment in lymph nodes not connected to the tumor (Fig. 3*F*).

Modulation of Tumor Microenvironment by NP Stimulation. We next evaluated the tumor microenvironment changes in the B16F10 tumors after NP treatment, as the composition and characteristics of the tumor microenvironment are thought to play an important role in determining the antitumor immune response. Luminex analysis of intratumoral cytokines and chemokines revealed significant up-regulation of proinflammatory cytokines and chemokines after NP treatment, demonstrating their capacity to modulate the tumor microenvironment from significantly suppressive conditions to inflammatory ones (Fig. 4*A*). The blank NPs failed to generate an immune-stimulating microenvironment such as that elicited by the fully loaded NPs, showing an indistinguishable cytokine signature from PBS (*SI Appendix*, Fig. S7). Since these secreted inflammatory cytokines and chemokines are critical for the activation of dendritic cells (DCs) and the recruitment of innate effectors and T cells into the tumor site, we then analyzed the phenotypic changes of cellular components in the tumor microenvironment. The results showed that the NPs were capable of facilitating the maturation of DCs and promoting their efficiency as APCs, as evident by the increased expression of major histocompatibility complex (MHC) class II (Fig. 4*B*). This observation is consistent with previous reports that DCs are pivotal for sensing microbial stimuli through TLRs and/or NOD-like receptors (30, 31). Notably, we observed a synergistic enhancement of cross-presentation of DCs and subsequent improvement in stimulating the proliferation of OT1-specific CD8$^+$ T cells by combining both Pam3CSK4 and L18-MDP in NPs (*SI Appendix*, Fig. S8*A*). The reason could be due, in part, to the NPs increasing the efficiency of TLR1/2 and NOD2 agonist uptake into DCs, providing broad access to the receptors expressed both on the cell surface and within the cytoplasm, thus eliciting a stronger adjuvant effect. This idea is supported by fluorescence-activated cell sorting (FACS) analysis, which shows a profound increase of fluorescence intensity in DCs after coincubation with NP-encapsulated rhodamine-labeled Pam3CSK4 and L18-MDP compared with those coincubated with soluble adjuvants (*SI Appendix*, Fig. S8 *B* and *C*).

After sensing these stimuli, the cytokines produced by DCs then played a critical role in orchestrating the subsequent development of T cell subsets (32). So, we next analyzed the phenotypic and functional changes of tumor-infiltrating CD4$^+$ T cells after NP treatment. Surprisingly, the data showed a marked down-regulation of Foxp3 expression of CD4$^+$ T cells contrasting with a significant increase in the frequency of IL-17–producing CD4$^+$ T cells (Th17 cells) in both B16F10 and MC38 models (Fig. 4*C*). Thus, NP treatment elicited a substantial remodeling of the tumor microenvironment with contributions from diverse immune cells, resulting in the activation of antigen-specific CD8$^+$ T cells.

Activation of Endogenous TILs in Human Tumor Organoids. To investigate the therapeutic potential of this strategy in human cancer therapy, we then tested NPs modified to stimulate human T cells in patient-derived tumor organoids, an in vitro culture system that generates from human surgically resected tumor biopsies and functionally recapitulates the tumor microenvironment and its endogenous infiltrating lymphocytes (33). After 7 d of continuous coculture with the organoids (only one organoid culture for each stimulation condition was set up due to the limited tumor biopsies) derived from three different cancer types, including renal cell carcinoma, lung cancer, and melanoma (*SI Appendix*, Table S3), these NPs stimulated a robust T cell response within the organoids, as evidenced by a marked increase in the number of CD3$^+$, CD4$^+$, and CD8$^+$ TILs (Fig. 5*A*) and a strong induction of the T cell cytotoxicity factor Granzyme B (GZMB; with 3- to 8-fold increases in RNA levels), Interferon-γ (IFNG; 4- to 17-fold increase), and Perforin-1 (PRF1; 2- to 12-fold increase) in FACS-sorted CD3$^+$

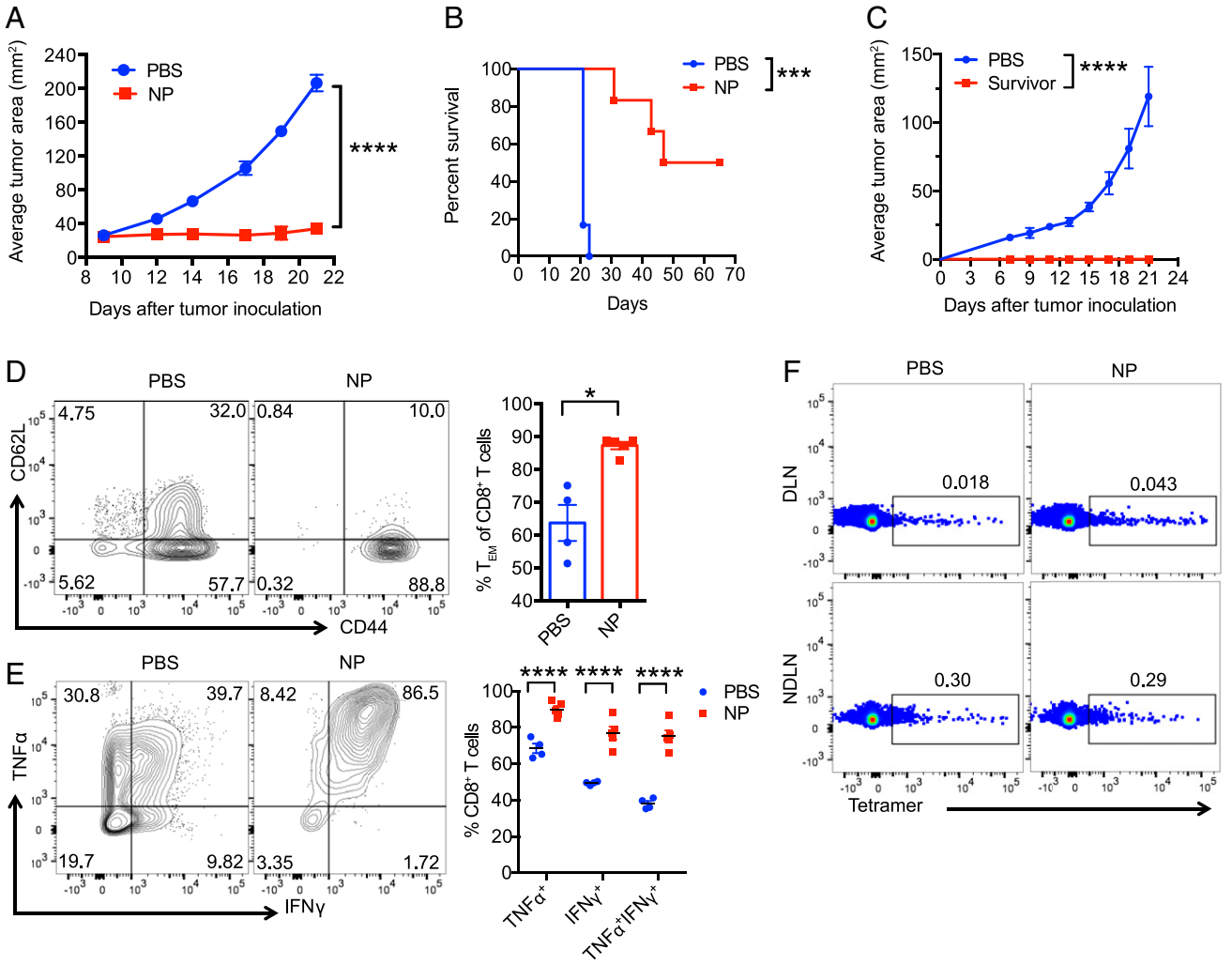

Fig. 3. Loaded NPs elicit a robust neoantigen-specific CD8$^+$ T cell response and trigger suppression of tumor growth, prolongation of overall survival, and establishment of protective memory in MC38 colon cancer model. (*A*) The average tumor growth curve of mice bearing MC38 cancer ($n = 6$) who received three injections of PBS or NPs on days 9, 14, and 19. Data were analyzed by two-way ANOVA. ****$P < 0.0001$. (*B*) The percentage survival of mice bearing the MC38 tumor line ($n = 6$) after three treatments was monitored over time. Data were analyzed by the log-rank (Mantel–Cox) test. ***$P < 0.001$. (*C*) The tumor growth curve of survivors bearing MC38 tumors ($n = 3$ for survivor; $n = 5$ for PBS control) who received a second tumor challenge on day 70. Data were analyzed by two-way ANOVA. ****$P < 0.0001$. (*D*) NP drives the endogenous CD8$^+$ T cell response strongly biased toward effector memory (T_{EM}: CD44^{hi}CD62L^{lo}CD8$^+$T) populations (flow plot [*Left*]; quantification [*Right*]; $n = 4$ to 5). Data were analyzed by unpaired *t* test with Welch's correction. *$P < 0.05$. (*E*) The representative flow cytometry plot (*Left*) and the corresponding quantification (*Right*) show that these NPs increase the frequency of TNF-α and IFN-γ–producing CD8$^+$ T cells in MC38 colon cancer on day 17 ($n = 4$ to 5). Data were analyzed by two-way ANOVA with Sidak's multiple comparison test. ****$P < 0.0001$. (*F*) Representative flow cytometric analysis showing the frequency of neoantigen (ASMTNMELM)-specific CD8$^+$ T cells in tumor-draining lymph nodes (DLNs) and nontumor-draining lymph nodes (NDLNs) of MC38 tumor-bearing mice after either PBS or NP injections.

TILs (Fig. 5*B*) compared with a human isotype Immunoglobulin G (IgG) control or therapeutic PD-1 checkpoint blocking Ab (Nivolumab). Importantly, the NPs strongly stimulated the CD8$^+$ TILs in the melanoma organoid, with remarkable up-regulation of CD69 and CD25 expression and a significant increase in the production of TNF-α and IFN-γ in these cells (Fig. 5*C*). In contrast, anti–PD-1 treatment induced only a negligible activation of these CD8$^+$ TILs vs. the IgG control. Luminex analysis of cytokines and chemokines in the melanoma organoid culture medium also showed significant increases in granulocyte–macrophage colony-stimulating factor (GMCSF) and IL-2, which have been used as immunostimulatory adjuvants in clinical studies to enhance the antitumor immune response (34, 35). Overall, these studies strongly suggest the NPs could profoundly activate and expand TILs in human tumor organoids, even those that are unresponsive to checkpoint blockade immunotherapy. We note that ultrasound-guided drug delivery methods (36) have been extensively tested in both preclinical and clinical studies, making it possible to deliver NPs directly to human tumors.

Discussion

Previously, we found that self-specific CD8$^+$ T cells from human peripheral blood could not be activated by their cognate peptides in vitro, in contrast to foreign antigen-specific ones (18). Here, we show that the addition of agonists for two PRRs, TLR1/2 and NOD2, is sufficient to stimulate self-specific T cells as efficiently as foreign antigen-specific ones, in the presence of their respective antigens plus IL-2 and CD28 stimulation in vitro. This reinforces and extends the earlier finding of Ohashi et al. (20) that T cell peripheral tolerance is typically broken during infection. There is

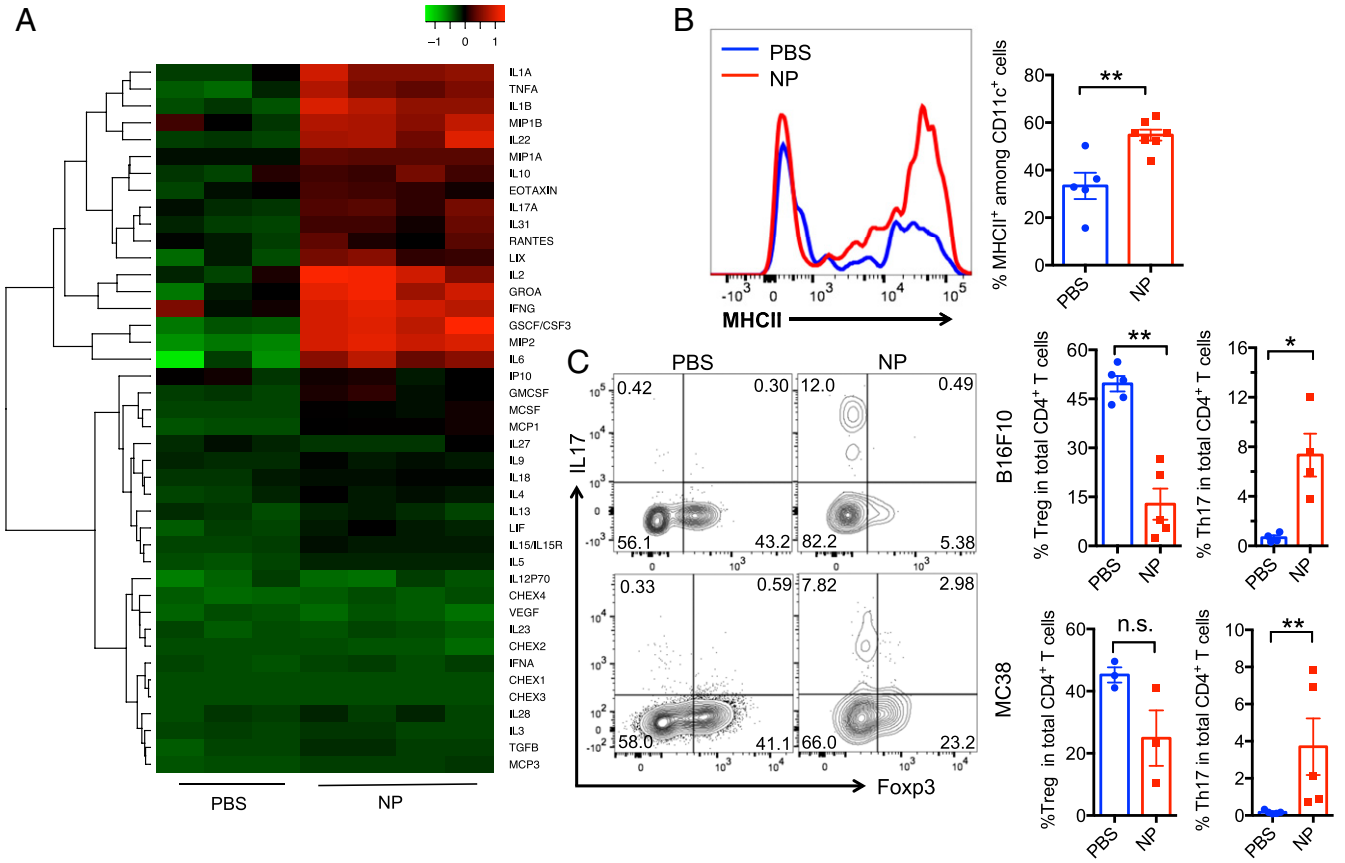

Fig. 4. Loaded NPs remodel the tumor microenvironment of established solid tumors and induce a potent endogenous T cell response in the B16F10 and MC38 tumor models. (*A*) Luminex analysis of the intratumoral cytokine and chemokine expression from B16F10 melanoma-bearing mice 3 d after a single treatment with PBS or NPs ($n = 4$). The data are represented as $\log_{10}$ fold change of mean fluorescence intensity over the PBS control. (*B*) NPs enhance the maturation of DCs. Representative flow cytometry plot of MHCII expression of $CD11c^+$ DCs (*Left*) and the quantification of the percentage of $MHCII^{hi}$ among $CD11c^+$ DCs ($n = 5$ to 7). Data are means ± SEM. $^{**}P < 0.01$ analyzed by the Mann–Whitney test. (*C*) Tumor-infiltrating $CD4^+$ T cells were isolated from B16F10 melanoma ($n = 4$ to 5) and MC38 colon carcinoma ($n = 3$ to 5) and stained for Foxp3 and IL-17 expression after ex vivo stimulation of cell stimulation mixture for 5 h on day 17. The representative flow plot is shown (*Left*), and the quantification of the Tregs (Treg $CD4^+Foxp3^+$ cells) and Th17 ($CD4^+IL\text{-}17^+$) cells in B16F10 melanoma and MC38 colon carcinoma is summarized (*Right*). All of data are means ± SEM. Data were analyzed by Mann–Whitney test. n.s., not significant. $^*P < 0.05$; $^{**}P < 0.01$.

also the example of the recently approved oncolytic virus treatment for melanoma (37, 38) and the much earlier finding of W. B. Coley that repeated injection of live *Streptococcus pyogenes* (erysipelas) or a heat-killed combination of *S. pyogenes* and *Serratia marcescens* (39) resulted in remarkable and durable antitumor responses in a significant number of sarcoma patients (40). This evidence is consistent with the view that instigating or mimicking an infectious disease response can overcome peripheral tolerance. Here, we identify the specific innate immune triggers necessary for this to occur, both in vitro and presumably in vivo, at least in the context of the tumor microenvironment analyzed here.

We also show here that this finding has significant relevance as a modality of cancer immunotherapy. In both mouse and human tumors, there is increasing evidence of self-antigen–specific $CD8^+$ T cells in tumor infiltrates (14, 21, 29). While there is much current attention on neoantigen approaches, many solid tumors have relatively low mutational burdens, such as hormone receptor-positive breast cancer, ovarian cancer, colon cancer, and so on. However, these self-specific T cells are often inactive (41), due to apparent suppression by regulatory $CD4^+$ T cells (42) and/or the induction of cell-intrinsic programs that force self-reactive T cells into a state of functional unresponsiveness (43, 44). The lack of a robust in vivo stimulation method makes it challenging to unleash their antitumor functions without exacerbating autoimmunity. Thus, we devised an NP-based stimulation method, which in vivo activates quiescent tumor-infiltrating self-reactive $CD8^+$ T cells through local and persistent innate stimulation via PRRs without inducing severe systemic adverse effects. This also has the advantage of not requiring any knowledge of specific antigens or their MHC restriction. Our data show that this stimulation method had a profound effect on the proliferation, cytokine production, and cell fate differentiation of $TRP2^+CD8^+$ TILs in the B16F10 melanoma, resulting in significant inhibition of tumor growth and prolongation of mouse survival. Interestingly, NP stimulation also induced a robust antitumor immune response in the MC38 colon cancer model, which carries a high tumor mutational burden. Indeed, $CD8^+$ T cells specific for at least one neoantigen are expanded in the tumor-draining lymph node from MC38-bearing mice after NP injection. Although neoantigens that arise as a consequence of tumor-specific mutations can be a major factor in stimulating an immune response (9, 45), the substantial variation in the composition of the tumor microenvironment will likely influence the ability of the T cells responding to these neoantigens. This is in line with the observation that neoantigen-specific TILs displayed a more exhausted phenotype characterized by increased expression of PD-1 and T cell immunoglobulin and mucin domain-containing protein 3 (Tim 3) than bulk $CD8^+$ TILs in certain cancer models (46, 47). Thus, we suggest that NPs can also stimulate neoantigen-specific TILs, likely because they are also subject

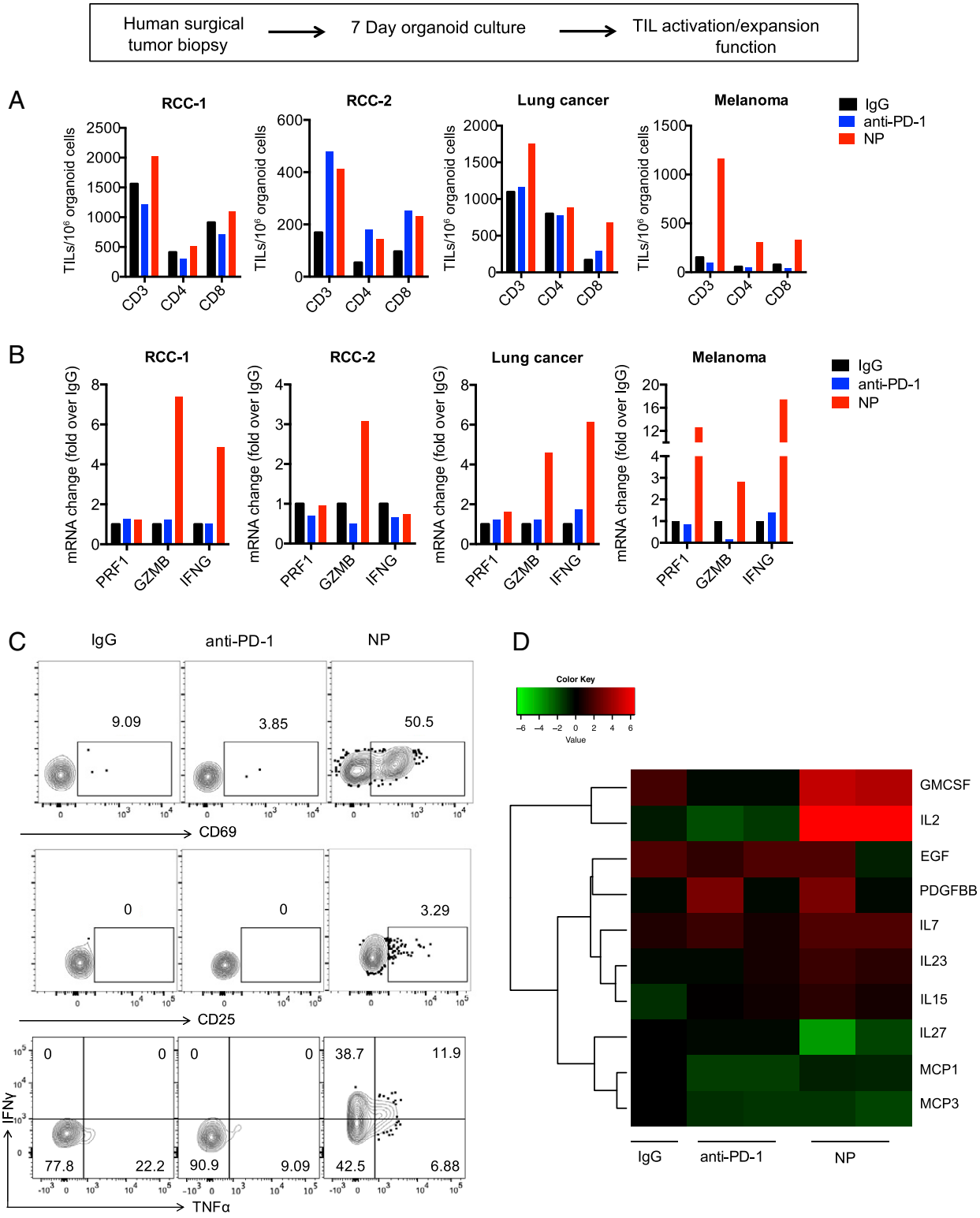

Fig. 5. Loaded NPs enable the robust activation and expansion of endogenous TILs in cancer organoids derived from surgical resections of renal cell, lung cancer, and melanoma tumors. (*A*) Quantification of live $CD3^+$, $CD4^+$, and $CD8^+$ TILs per 10^6 organoid cells by FACS analysis after 7-d IgG, anti–PD-1, or NP treatment. (*B*) qRT-PCR quantification of messenger RNA (mRNA) of *IFNG*, *PRF*, and *GZMB* of FACS-sorted $CD3^+$ TILs from patient-derived organoids (PDOs) after 7-d IgG, anti–PD-1, or NP treatment. (*C*) The expression of CD69 and CD25 of $CD8^+$ TILs in 7-d cultured melanoma organoids and their production of TNF-α and IFN-γ after ex vivo stimulation with the cell stimulation mixture for 3 h. The flow cytometry plots shown are gated on live $CD3^+CD8^+$ TILs. (*D*) Luminex analysis of the cytokine and chemokine expression from the melanoma organoid culture medium ($n = 2$ technical replicates for Luminex analysis). The data are represented as $\log_2$ fold change of the cytokine concentration over IgG-treated organoids.

to peripheral tolerance. The tumor organoid data show that our NPs can also stimulate human T cells in that context and thus, are not confined to the mouse tumor models described here. The ongoing single-cell analysis study will also provide more insights into whether these NPs only reactivate the previously tolerized cells or allow new cells to infiltrate into the NP-modified tumor environment resistant to tolerance. Overall, the NP stimulation approach described here represents a broadly applicable cancer immunotherapeutic strategy. Compared with the current personalized cancer vaccine development based on the discovery of patient-specific mutations, this could be more time efficient and cost effective in clinical settings.

Several studies have indicated that TIL dysfunction is a unique status distinct from T cell exhaustion (41, 48). Both self-specific and neoantigen-specific TILs examined in this study were activated upon NP stimulation, suggesting that both types of TILs are subject to peripheral tolerance (20, 49) but can be switched in vivo to effector cells with an optimized combination of stimuli. This reprogramming process is, at least in part, due to an imbalance between Th17 cells and Tregs as well as the condition of DCs. In the suppressive tumor microenvironment, an incomplete form of DC maturation generates a tolerogenic DC. Self-peptide-major histocompatibility complex complexes on tolerogenic DCs induced the induction of factors including PD-1. They subsequently maintained T cells in an unresponsive state, in part by inhibiting stable interactions with DCs and preventing further TCR engagement. Moreover, mutual interactions between DCs and Tregs are thought to maintain peripheral tolerance; tolerogenic DCs induce Tregs, and conversely, Tregs prepare DCs for an immunosuppressive role, thus extending the immunosuppressive function of Tregs. Based on the data presented here, we postulate that NP-enabled persistent intratumoral stimulation can break this tolerance by promoting the maturation of DCs as well as reducing the number of Tregs and inducing Th17 cells. This is in agreement with the previous reports that persistent TLR1/2 signaling can reduce the suppressive functions of Tregs (50, 51). It also has been shown TLR1/2 ligand, in combination with NOD2 ligand, can activate DCs to selectively trigger a Th17-polarizing program (52). Therefore, by tuning the release kinetics of TLR1/2 ligand (Pam3CSK4) and NOD2 ligand (L18-MDP), the NPs offered the possibility to maintain their concentration within the therapeutic window at the tumor site, in order to continuously regulate the balance between Tregs and Th17 cells, thus overcoming Treg-mediated suppression on both DCs and $CD8^+$ T cells. The persistent local up-regulation of proinflammatory cytokines induced by NP stimulation stimulates DCs to render self-specific $CD8^+$ T cells refractory to Treg-mediated suppression and keeps self-specific effector memory T cells efficiently retained at tumor sites with high antigen expression through continuous TCR ligation.

Compared with the repeated local injection of soluble stimulants, the NP strategy used here offers several unique advantages. First, the NPs we have formulated enable a slow release of IL-2 and the two PRR agonists (*SI Appendix*, Fig. S2 *B* and *C*). In contrast, subcutaneous injection of a soluble stimulant mixture of IL-2, the two PRR agonists, and anti-CD28 Ab leaked into the serum within 2 h, causing substantial elevation of IL-6 in the serum (Fig. 1*C*). This systemic leakage will limit the possible clinical dosages of stimulants due to undesired toxicity. Also, the fast escape of the locally injected soluble stimulant mixture out of the tumor also failed to prolong the intratumoral persistence of TLR signaling necessary for reversing Treg-mediated CD8 T cell tolerance (50). Second, loading a TLR1/2 ligand and an NOD2 ligand into a single NP platform may enable the simultaneous triggering of surface TLR1/2 signaling and endosomal NOD2 signaling in the same DC population, synergistically converting them to matured APCs for eliciting subsequent T cell response. Third, the NP approach helps keep the stimulants needed to overcome tolerance localized in the tumor, limiting the risk of autoimmunity, as there is no sign of any obvious pathology observed in the study.

Overall, our set of results basically creates a paradigm and treatment logic for cancer immunotherapy—that specific innate immune signals are needed to overcome peripheral tolerance in TILs with a broad range of both self- and neoantigen specificities.

Materials and Methods

Abs. All Abs were purchased from BD Bioscience, BioLegend, or ebioscience. The following Abs were used in the study: anti-CD16/CD32 (BD Bioscience; catalog no. 553141, clone 2.4G2), Brilliant Violet 785 anti-mouse CD45 (BioLegend; catalog no. 103149, clone 30-F11), PE/Dazzle 594 anti-mouse TCRb chain (catalog no. 109240, clone H57-597), APC-Cy7 anti-mouse CD3 (BioLegend; catalog no. 100330, clone 145-2C11), PerCP-Cy5.5 anti-mouse CD8α (BioLegend; catalog no. 100734, clone 53-6.7), Pacific Blue anti-mouse CD4 (BioLegend; catalog no. 100428, clone GK1.5), anti-mouse CD11c fluorescein isothiocyanate (FITC) (ebioscience; lot: E00154-1631, clone N418), anti-mouse F4/80 APC (ebioscience; lot: 4271644, clone BM8), Brilliant Violet 421 anti-mouse CD25 (BioLegend; catalog no. 102043, clone PC61), APC anti-mouse/human CD44 (BioLegend; catalog no. 103012, clone IM7), Brilliant Violet 605 anti-mouse CD62L (BioLegend; catalog no. 104438, clone MFL-14), PE/Cy7 anti-mouse CD69 (BioLegend; catalog no. 104512, clone H1.2F3), Alexa Fluor 488 anti-mouse Foxp3 (Biolegend; catalog no. 126406, clone MF-14), APC anti-mouse IL-17A (BioLegend; catalog no. 506916, clone TC11-18 H10.1), Brilliant Violet 711 anti-mouse CD279 (PD-1; BioLegend; catalog no. 135231, clone 29F.1A12), BD Pharmingen FITC rat anti-mouse TNF (BD Biosciences; catalog no. 554418), BD Pharmingen PE-Cy7 rat anti-mouse IFN-γ (BD Biosciences; catalog no. 557649, clone XMG 1.2), FITC anti-human CD45 (BD Biosciences; catalog no. 340664, clone 2D1), PE anti-human CD3 (BD Biosciences; catalog no. 555333, clone UCHT1), BV605 anti-human CD4 (BD Biosciences; catalog no. 562658, clone RPA-T4), BV786 anti-human CD8 (BD Biosciences; catalog no. 563823, clone RPA-T8), APC/Cy7 anti-human CD69 (BioLegend; catalog no. 310914, clone FN50), PE/Dazzle 594 anti-human CD25 (BioLegend; catalog no. 302646, clone BC96), BUV 805 anti-human CD8 (BD Biosciences; catalog no. 564912, clone SK1), Alexa Fluor 700 anti-human CD3 (BioLegend; catalog no. 300324, clone UCHT1), Brilliant Violet 650 anti-human CD4 (BioLegend; catalog no. 300536, clone RPA-T4), Pacific Blue anti-human TNF-α (BioLegend; catalog no. 502920, clone MAb11), and phycoerythrin (PE) anti-human IFN-γ (BioLegend; catalog no. 502510, clone 4S.B3).

Instrument. The sizes and the size distributions of the NPs were determined on a ZetaPALS dynamic light scattering detector (15-mW laser, incident beam = 676 nm; Brookhaven Instruments). Lyophilization of the NPs was carried out on a benchtop lyophilizer (FreeZone 2.5; Fisher Scientific). Flow data were acquired on an LSRII or LSRII.2 flow cytometer (BD Biosciences). Cells were sorted on FACSAria Fusion (BD Biosciences). The absorbance of enzyme-linked immunosorbent assay (ELISA) and the fluorescence intensity of rhodamine-labeled Pam3CSK4 and MDP were measured on The FlexStation 3 Multi-Mode Microplate Reader (Molecular Devices). qRT-PCR was performed on a StepOnePlus instrument (Applied Biosystems).

Cell Culture. B16F10 cells were purchased from American Type Culture Collection (ATCC) and cultured in Dulbecco's Modified Eagle Medium (DMEM) containing 10% fetal bovine serum (FBS) and 100 units/mL aqueous Penicillin G sodium and 100 μg/mL streptomycin (Pen/Strep) at 37 °C in 5% CO_2 humidified air. JAWSII cells were purchased from ATCC and cultured in alpha minimum essential medium with ribonucleosides, deoxyribonucleosides, 4 mM L-glutamine, 1 mM sodium pyruvate, and 5 ng/mL murine GMCSF, 80%; FBS, 20%. MC38 cells were purchased from Kerafast, Inc. and cultured in DMEM containing 10% FBS, 2 mM glutamine, 0.1 mM nonessential amino acids, 1 mM sodium pyruvate, 10 mM 4-(2-hydroxyethyl)-1-piperazineethanesulfonic acid (Hepes), 50 μg/mL gentamycin sulfate, Pen/Strep. TLR2 reporter cell line RAW-Blue cells were purchased from Invivogen and cultured in DMEM containing 10% FBS, 100 mg/mL Normocin, 2 mM glutamine, and 200 μg/mL Zeocin.

Animals. Six- to 8-wk-old female C57BL/6J mice were purchased from the Jackson Laboratory. All the animals were cared for in the Stanford Animal Facility under federal, state, and NIH guidelines. The study protocol was reviewed and approved by the University Administrative Panel on Laboratory Animal Care.

Human Samples. Human PBMCs were obtained from platelet apheresis donors through the Stanford Blood Bank according to Institutional Review Board (IRB) protocol. Human tumor tissues were obtained through the Stanford

Tissue Bank derived from patients undergoing surgical tumor resection at Stanford University Medical Center (SUMC). Human specimen collection was approved by the SUMC Institutional Review Board and performed under the approved protocol. Written informed consent was obtained from donors prior to tissue acquisition from treatment-naïve adult male or female patients. These samples were deidentified prior to use in this study.

In vitro stimulation/proliferation of human self- and foreign-specific CD8⁺ T cells. For the proliferation assay, $CD8^+$ T cells were concentrated from the human platelet donors and then sorted by pooled HLA-A*0201 tetramers loaded with self- or foreign-specific peptides (Table 1). Approximately 500 cells were sorted, carboxyfluorescein succinimidyl ester (CFSE) labeled, and cultured under the various stimulation conditions: 1) peptide (1.5 μg/mL) and anti-CD28 Ab (10 μg/mL); 2) peptide (1.5 μg/mL), IL-2 (75 IU), Pam3CSK4 (5 μg/mL), L18-MDP (5 μg/mL), and anti-CD28 Ab (10 μg/mL); and 3) peptide (1. 5μg/mL) and NPs (equivalent dose as soluble cytokine) in the presence of ∼750,000 autologous PBMCs in RPMI media with 10% FBS, 100 U/mL Pen/Strep, and glutamine supplement for 7.5 d. The proliferation was characterized by measuring the CFSE dilution of $tetramer^+CD8^+$ T cells. For the activation assay, PBMCs were directly cultured in the presence of pooled peptides and stained with pooled HLA-A*0201 tetramers at day 7.5. The activation was characterized by measuring CD25 expression of $tetramer^+CD8^+$ T cells.

Ex vivo expansion of TRP2-specific CD8⁺ T cells. Female C57BL/6 mice (6 to 8 wk) were anesthetized and inoculated subcutaneously onto the right flank with 1×10^5 B16F10 murine melanoma tumor cells. When the tumor was established (∼8 × 8 mm), the tumor-draining lymph nodes were dissected to prepare single-cell suspensions. The cells were washed and labeled with the CellTrace Far Red Cell (CTFR) Proliferation Kit (Invitrogen) as well as stained with LIVE/DEAD Fixable Aqua Dead Cell Stain and surface markers (CD45, CD3, TCRb, CD4, CD8) for FACS sorting. Approximately 6,000 live $CD3^+TCRb^+CD8^+$ cells were sorted and plated per well in a 96-well U-bottom plate with 15,000 JAWSII cells per well and cultured using complete RPMI1640 medium (RPMI1640 containing 10% FBS, Pen/Strep, sodium pyruvate, and β-mercaptoethanol) in the presence of various stimuli: 1) anti-mouse CD3 Ab (1 μg/mL) plus anti-mouse CD28 Ab (2 μg/mL); 2) $TRP2_{180–188}$ peptide (SVYDFFVWL; 10 μg/mL) and anti-mouse CD28 Ab (2 μg/mL); 3) $TRP2_{180–188}$ peptide (SVYDFFVWL) and full loaded NPs (equivalent dose: IL-2 [16 ng/mL], Pam3CSK4 [1 μg/mL], L18-MDP [1 μg/mL], anti-CD28 Ab [2 μg/mL]); and 4) a series of NPs with one component excluded (*SI Appendix*, Table S1) for 5 d. Cells were collected and stained with Aqua, CD3, CD4, and CD8 and analyzed by Flowjo software. The extent of CTFR-labeled TRP2-specific $CD8^+$ T cells was analyzed by calculating CTFR dilution.

Serum cytokine measurements. Female C57BL/6 mice (6 to 8 wk) were injected subcutaneously with PBS, NPs, and a soluble cytokine mixture (equivalent dose per mouse: 160 ng IL-2, 10 μg Pam3CSK4, 10 μg L18-MDP, and 20 μg anti-CD28 Ab). Blood was collected 2 h postinjection. IL-6 in the serum was measured using a Luminex bead-based ELISA following the manufacturer's instructions.

Splenomegaly measurements. Female C57BL/6 mice (6 to 8 wk) were injected subcutaneously with PBS, NPs, and a soluble cytokine mixture at day 1, day 3, and day 5 (equivalent dose per mouse: 160 ng IL-2, 10 μg Pam3CSK4, 10 μg L18-MDP, and 20 μg anti-CD28 Ab). Spleens were collected and weighted at day 7 after three injections.

Tumor efficacy study. Female C57BL/6 mice (6 to 8 wk) were anesthetized and inoculated subcutaneously onto the right flank with 1×10^5 B16F10 murine melanoma tumor cells or 5×10^5 MC38 murine colon cancer cells. On day 5 (for B16F10) or day 9 (for MC38), mice with established tumors were randomly divided into groups, minimizing weight and tumor size difference among the groups. B16F10 tumor-bearing mice were treated three times on day 5, day 11, and day 17 through intratumoral injection of PBS (1×, 50 μL) and NPs (equivalent dose per mouse: 160 ng IL-2, 10 μg Pam3CSK4, 10 μg L18-MDP, and 20 μg anti-CD28 Ab). MC38 tumor-bearing mice were treated three times on day 9, day 14, and day 19 through intratumoral injection of PBS (1×, 50 μL) and stimulatory PLGA NPs (equivalent dose per mouse: 160 ng IL-2, 10 μg Pam3CSK4, 10 μg L18-MDP, and 20 μg anti-CD28 Ab). The body weight and tumor sizes of animals were monitored every 2 or 3 d. The tumor sizes were monitored by calipers and calculated according to the formula (length) × (width). If body weight loss is beyond 20% of predosing weight, the animals were euthanized. When the tumor load reached 150 mm^2 (as the predetermined end point) or the animal had become moribund, the mouse was euthanized.

Tetramer staining and phenotype analysis. Female C57BL/6 mice (6 to 8 wk) were anesthetized and inoculated subcutaneously onto the right flank with 1×10^5 B16F10 murine melanoma or 5×10^5 MC38 murine colon cancer cells. When the tumor was established, mice were intratumorally injected with PBS or NPs (same dose as the tumor efficacy study; B16F10 melanoma at day 5 and day 11; MC38 colon cancer at day 7 and day 12). B16F10 or MC38 tumors were harvested at day 17 and cut into small pieces. The tumor pieces were digested in 2 mL RPMI 1640 containing FBS (2%), Collagenese D (1 mg/mL), and DNAese (10 μg/mL) at 37 °C for 1 h. Then, 2 μL ethylenediaminetetraacetic acid (0.5 M) was added into the digestion solution, and the digestion solution went through the cell strainer (70 μm) to prepare a single-cell suspension. The cells were washed and blocked with Fc blocker (anti-mouse CD16/CD32 monoclonal Ab on ice for 10 min). Then, cells were stained with PE-labeled H2-K^b-TRP2 tetramer (MBL International Corporation) or customized H2-D^b-ASMTNMELM tetramer and incubated at room temperature for 1 h. Cells were washed twice, then stained with LIVE/DEAD Fixable Aqua Dead Cell Stain and surface markers (CD45, CD3, TCRb, CD4, CD8, CD44, CD62L, CD69, CD25, PD-1, CD11b, CD11c, F4/80, MHCII), and analyzed on a BD LSRII flow cytometer.

Functional analysis of TILs. The tumor single-cell suspension was prepared as above described. For antigen-specific stimulation, the cells were plated in 24-well plates and pulsed with $TRP2_{180–188}$ (SVYDFFVWL) for 16 h at 37 °C in complete T cell media (RPMI 1640, 10% FBS, 50 μM β-mercaptoethanol, 100 U/mL Pen/Strep, 1× MEM Non Essential Amino Acids Solution, 1 mM sodium pyruvate) with ebioscience Protein Transport Inhibitor Mixture. For broad stimulation, the cells were plated in 24-well plates in complete T cell media with ebioscience Cell Stimulation Mixture (plus protein transport inhibitors) for 5 h. After stimulation, the cells were collected, washed, blocked with Fc blocker, stained with LIVE/DEAD Fixable Aqua Dead Cell Stain and surface markers (CD45, CD3, TCRb, CD4, CD8), and then fixed using the ebioscience Foxp3/Transcription Factor Staining Buffer Set according to the manufacturer's instructions. Cells were then washed and permeabilized for intracellular staining for IFN-γ, TNF-α, Foxp3, and IL-17. Then, cells were analyzed on a BD LSRII flow cytometer.

Intratumoral cytokine measurements. Female C57BL/6 mice (6 to 8 wk) were anesthetized and inoculated subcutaneously onto the right flank with 1×10^5 B16F10 murine melanoma tumor cells. When the tumor was established, mice were intratumorally injected with PBS and NPs (same dose as the tumor efficacy study). Tumors were harvested 3 d postinjection and prepared as the single-cell suspension as above described. The suspension was centrifuged at 4,000 rpm for 10 min. The supernatant was aliquoted and stored at −80 °C until analysis. Samples were diluted 1:1 with Assay Buffer and assayed using a Luminex bead-based ELISA following the manufacturer's instructions.

Generation of tumor organoids and TIL analysis. Human tumor tissues were collected, minced on ice, washed twice in Advanced Dulbecco's Modified Eagle Medium/Nutrient Mixture (ADMEM/F12) (Invitrogen) containing 1× Normocin (InvivoGen), and resuspended in 1 mL of Type I collagen gel (Trevigen). They were then layered on top of presolidified 1 mL collagen gel within a 30-mm, 0.4-μm inner transwell, which forms the double-dish air–liquid culture system as previously described (33) The tumor tissue in the transwell was placed into an outer 60-mm cell culture dish containing 1.0 mL of medium (ADMEM/F12 supplemented with 50% Wnt3a, R-spondin1, Noggin-conditioned media [L-WRN; ATCC] with Hepes [1 mM; Invitrogen], Glutamax [1×; Invitrogen], Nicotinamide [10 mM; Sigma], *N*-acetylcysteine [1 mM; Sigma], B-27 without vitamin A [1×; Invitrogen], A83-01 [0.5 μM; Tocris], Pen/Strep Glutamine [1×; Invitrogen], Gastrin [10 nM; Sigma], and epidermal growth factor [50 ng/mL; Invitrogen]) followed by replacing the lid of the outer dish. For in vitro treatment of human tumors with different therapies, established organoid cultures were supplemented with organoid medium containing NPs (75 IU IL-2, 5 μg/mL Pam3CSK4, 5 μg/mL L18-MDP, 10 μg/mL anti-human CD28 Ab), 10 μg/mL nivolumab (Bristol-Myers Squibb), or 10 μg/mL control human IgG4 (BioLegend). Organoids were grown for 7 d, and the supernatant from organoid culture was taken out for quantification of cytokines and chemokines by Luminex assay. The organoid was dissociated in 200 units mL^{-1} collagenase IV (Worthington) at 37 °C for 30 min, washed twice in ADMEM/F12, digested in Liberase-TL (Roche; 50 μg/mL final concentration) at 37 °C for 15 min, and then prepared further for FACS. The live $CD3^+$ TILs were sorted with a BD Aria II flow cytometer into RNA extraction buffer, and RNA was extracted using the Arcturus PicoPure kit (Applied Biosystems). Extracted RNA was converted to complementary DNA (cDNA) using the iScript cDNA synthesis kit (Bio-Rad), and cDNA was preamplified using SsoAdvanced PreAmp Supermix (Bio-Rad). cDNA was used for quantitative real-time PCR on a StepOnePlus instrument (Applied Biosystems) using TaqMan probe/primer sets for TATA-binding protein, IFNG, GZMB, and PRF1 (Applied Biosystems). For the melanoma organoid sample, part of the single-cell suspension was stimulated with ebioscience Cell Stimulation Mixture (plus protein transport inhibitors; Thermo Fisher Scientific) at 37 °C for 3 h. Then, cells were collected and stained for intracellular cytokine analysis of TNF-α and IFN-γ.

Data Availability. All study data are included in the article and/or *SI Appendix*.

ACKNOWLEDGMENTS. We thank the Stanford Nano Shared Facilities, the Stanford Shared fluorescence-activated cell sorting (FACS) Facility, and The Human Immune Monitoring Center at Stanford for assistance in these experiments, and members of the laboratory of M.M.D. for helpful advice and discussion. We also thank Ning Cheng and Michitaka Nakano in the laboratory of C.J.K. for helping with some tumor organoid experiments. We are grateful for the support of the HHMI, an NIH National Cancer Institute, The Center for Cancer Nanotechnology Excellence for Translational Diagnostics (NCI CCNE-TD) pilot grant (to Q.Y. and M.M.D.), and The Parker Institute for Cancer Immunotherapy (M.M.D.). We also thank the Emerson Collective for support (C.J.K.) and appreciate NIH Grants U54CA224081 (to C.J.K.) and U01CA217851 (to C.J.K.). Q.Y. was supported by a Cancer Research Institute Irvington Postdoctoral Fellowship and the Lloyd J. Old Memorial Fellowship from the Cancer Research Institute.

1. D. N. Khalil, E. L. Smith, R. J. Brentjens, J. D. Wolchok, The future of cancer treatment: Immunomodulation, CARs and combination immunotherapy. *Nat. Rev. Clin. Oncol.* **13**, 273–290 (2016).
2. D. M. Pardoll, The blockade of immune checkpoints in cancer immunotherapy. *Nat. Rev. Cancer* **12**, 252–264 (2012).
3. F. Teng, X. Meng, L. Kong, J. Yu, Progress and challenges of predictive biomarkers of anti PD-1/PD-L1 immunotherapy: A systematic review. *Cancer Lett.* **414**, 166–173 (2018).
4. A. Ribas, J. D. Wolchok, Cancer immunotherapy using checkpoint blockade. *Science* **359**, 1350–1355 (2018).
5. S. Gill, C. H. June, Going viral: Chimeric antigen receptor T-cell therapy for hematological malignancies. *Immunol. Rev.* **263**, 68–89 (2015).
6. W. H. Fridman, L. Zitvogel, C. Sautès-Fridman, G. Kroemer, The immune contexture in cancer prognosis and treatment. *Nat. Rev. Clin. Oncol.* **14**, 717–734 (2017).
7. D. S. Thommen, T. N. Schumacher, T cell dysfunction in cancer. *Cancer Cell* **33**, 547–562 (2018).
8. A. N. Houghton, J. A. Guevara-Patiño, Immune recognition of self in immunity against cancer. *J. Clin. Invest.* **114**, 468–471 (2004).
9. M. Efremova, F. Finotello, D. Rieder, Z. Trajanoski, Neoantigens generated by individual mutations and their role in cancer immunity and immunotherapy. *Front. Immunol.* **8**, 1679 (2017).
10. Y. Simoni *et al*., Bystander $CD8^+$ T cells are abundant and phenotypically distinct in human tumour infiltrates. *Nature* **557**, 575–579 (2018).
11. W. Scheper *et al*., Low and variable tumor reactivity of the intratumoral TCR repertoire in human cancers. *Nat. Med.* **25**, 89–94 (2019).
12. P. P. Lee *et al*., Characterization of circulating T cells specific for tumor-associated antigens in melanoma patients. *Nat. Med.* **5**, 677–685 (1999).
13. M. B. Bloom *et al*., Identification of tyrosinase-related protein 2 as a tumor rejection antigen for the B16 melanoma. *J. Exp. Med.* **185**, 453–459 (1997).
14. M. R. Parkhurst *et al*., Identification of a shared HLA-A*0201-restricted T-cell epitope from the melanoma antigen tyrosinase-related protein 2 (TRP2). *Cancer Res.* **58**, 4895–4901 (1998).
15. H. von Boehmer, Developmental biology of T cells in T cell-receptor transgenic mice. *Annu. Rev. Immunol.* **8**, 531–556 (1990).
16. H. von Boehmer, H. S. Teh, P. Kisielow, The thymus selects the useful, neglects the useless and destroys the harmful. *Immunol. Today* **10**, 57–61 (1989).
17. L. F. Su, B. A. Kidd, A. Han, J. J. Kotzin, M. M. Davis, Virus-specific CD4(+) memory-phenotype T cells are abundant in unexposed adults. *Immunity* **38**, 373–383 (2013).
18. W. Yu *et al*., Clonal deletion prunes but does not eliminate self-specific αβ CD8(+) T lymphocytes. *Immunity* **42**, 929–941 (2015).
19. F. P. Legoux *et al*., CD4+ T cell tolerance to tissue-restricted self antigens is mediated by antigen-specific regulatory T cells rather than deletion. *Immunity* **43**, 896–908 (2015).
20. P. S. Ohashi *et al*., Ablation of "tolerance" and induction of diabetes by virus infection in viral antigen transgenic mice. *Cell* **65**, 305–317 (1991).
21. M. H. Gee *et al*., Antigen identification for orphan T cell receptors expressed on tumor-infiltrating lymphocytes. *Cell* **172**, 549–563.e16 (2018).
22. A. Han, J. Glanville, L. Hansmann, M. M. Davis, Linking T-cell receptor sequence to functional phenotype at the single-cell level. *Nat. Biotechnol.* **33**, 210 (2015).
23. C. Yee *et al*., Melanocyte destruction after antigen-specific immunotherapy of melanoma: Direct evidence of T cell-mediated vitiligo. *J. Exp. Med.* **192**, 1637–1644 (2000).
24. M. T. Lotze *et al*., Clinical effects and toxicity of interleukin-2 in patients with cancer. *Cancer* **58**, 2764–2772 (1986).
25. T. Vial, J. Descotes, Clinical toxicity of interleukin-2. *Drug Saf.* **7**, 417–433 (1992).
26. D. M. Richards, B. Kyewski, M. Feuerer, Re-examining the nature and function of self-reactive T cells. *Trends Immunol.* **37**, 114–125 (2016).
27. R. L. McCall, R. W. Sirianni, PLGA nanoparticles formed by single- or double-emulsion with vitamin E-TPGS. *J. Vis. Exp.* **82**, e51015 (2013).
28. J. Azzi *et al*., Targeted delivery of immunomodulators to lymph nodes. *Cell Rep.* **15**, 1202–1213 (2016).
29. J. A. McWilliams, S. M. McGurran, S. W. Dow, J. E. Slansky, R. M. Kedl, A modified tyrosinase-related protein 2 epitope generates high-affinity tumor-specific T cells but does not mediate therapeutic efficacy in an intradermal tumor model. *J. Immunol.* **177**, 155–161 (2006).
30. T. H. Mogensen, Pathogen recognition and inflammatory signaling in innate immune defenses. *Clin. Microbiol. Rev.* **22**, 240–273 (2009).
31. V. Pavot *et al*., Cutting edge: New chimeric NOD2/TLR2 adjuvant drastically increases vaccine immunogenicity. *J. Immunol.* **193**, 5781–5785 (2014).
32. J. Zhu, H. Yamane, W. E. Paul, Differentiation of effector CD4 T cell populations (*). *Annu. Rev. Immunol.* **28**, 445–489 (2010).
33. J. T. Neal *et al*., Organoid modeling of the tumor immune microenvironment. *Cell* **175**, 1972–1988.e16 (2018).
34. G. C. de Gast *et al*., Phase I trial of combined immunotherapy with subcutaneous granulocyte macrophage colony-stimulating factor, low-dose interleukin 2, and interferon alpha in progressive metastatic melanoma and renal cell carcinoma. *Clin. Cancer Res.* **6**, 1267–1272 (2000).
35. W. L. Yan, K. Y. Shen, C. Y. Tien, Y. A. Chen, S. J. Liu, Recent progress in GM-CSF-based cancer immunotherapy. *Immunotherapy* **9**, 347–360 (2017).
36. Y. J. Bae, Y. I. Yoon, T. J. Yoon, H. J. Lee, Ultrasound-guided delivery of siRNA and a chemotherapeutic drug by using microbubble complexes: In vitro and in vivo evaluations in a prostate cancer model. *Korean J. Radiol.* **17**, 497–508 (2016).
37. L. Russell, K. W. Peng, The emerging role of oncolytic virus therapy against cancer. *Linchuang Zhongliuxue Zazhi* **7**, 16 (2018).
38. H. L. Kaufman, F. J. Kohlhapp, A. Zloza, Oncolytic viruses: A new class of immunotherapy drugs. *Nat. Rev. Drug Discov.* **14**, 642–662 (2015).
39. S. A. Hoption Cann, J. P. van Netten, C. van Netten, Dr William Coley and tumour regression: A place in history or in the future. *Postgrad. Med. J.* **79**, 672–680 (2003).
40. A. Anastasiadis, T. M. de Reijke, Best practice in the treatment of nonmuscle invasive bladder cancer. *Ther. Adv. Urol.* **4**, 13–32 (2012).
41. A. Schietinger *et al*., Tumor-specific T cell dysfunction is a dynamic antigen-driven differentiation program initiated early during tumorigenesis. *Immunity* **45**, 389–401 (2016).
42. K. Wing, S. Sakaguchi, Regulatory T cells exert checks and balances on self tolerance and autoimmunity. *Nat. Immunol.* **11**, 7–13 (2010).
43. A. Schietinger, P. D. Greenberg, Tolerance and exhaustion: Defining mechanisms of T cell dysfunction. *Trends Immunol.* **35**, 51–60 (2014).
44. W. L. Redmond, B. C. Marincek, L. A. Sherman, Distinct requirements for deletion versus anergy during CD8 T cell peripheral tolerance in vivo. *J. Immunol.* **174**, 2046–2053 (2005).
45. T. N. Schumacher, R. D. Schreiber, Neoantigens in cancer immunotherapy. *Science* **348**, 69–74 (2015).
46. M. Yadav *et al*., Predicting immunogenic tumour mutations by combining mass spectrometry and exome sequencing. *Nature* **515**, 572–576 (2014).
47. M. Fehlings *et al*., Checkpoint blockade immunotherapy reshapes the high-dimensional phenotypic heterogeneity of murine intratumoural neoantigen-specific $CD8^+$ T cells. *Nat. Commun.* **8**, 562 (2017).
48. A. Schietinger, J. J. Delrow, R. S. Basom, J. N. Blattman, P. D. Greenberg, Rescued tolerant CD8 T cells are preprogrammed to reestablish the tolerant state. *Science* **335**, 723–727 (2012).
49. K. Kawai, P. S. Ohashi, Immunological function of a defined T-cell population tolerized to low-affinity self-antigens. *Nature* **378**, 68–69 (1995).
50. Y. Yang, C. T. Huang, X. Huang, D. M. Pardoll, Persistent Toll-like receptor signals are required for reversal of regulatory T cell-mediated CD8 tolerance. *Nat. Immunol.* **5**, 508–515 (2004).
51. M. H. Nyirenda *et al*., TLR2 stimulation drives human naive and effector regulatory T cells into a Th17-like phenotype with reduced suppressive function. *J. Immunol.* **187**, 2278–2290 (2011).
52. A. J. van Beelen *et al*., Stimulation of the intracellular bacterial sensor NOD2 programs dendritic cells to promote interleukin-17 production in human memory T cells. *Immunity* **27**, 660–669 (2007).